**Preferred citation:** J.A. Olson, T.J. Ruth and R.J. Kerekes. Characterizing the Mobility of Papermaking Fibres During Sedimentation. In **The science of papermaking**, *Trans. of the XIIth Fund. Res. Symp. Oxford, 2001*, (C.F. Baker, ed.), pp 225–254, FRC, Manchester, 2018. DOI: 10.15376/frc.2001.1.225.

# CHARACTERIZING THE MOBILITY OF PAPERMAKING FIBRES DURING SEDIMENTATION

*D.M. Martinez*,[1,4] *K. Buckley*,[2] *S. Jivan*,[2]
*A. Lindström*,[1,4] *R. Thiruvengadaswamy*,[1,4] *J.A. Olson*,[3,4]
*T.J. Ruth*[2] *and R.J. Kerekes*[1,4]

[1]Department of Chemical and Bio-Resource Engineering, University of British Columbia
2216 Main Mall Vancouver BC Canada V6T 1Z4
[2]TRIUMF, University of British Columbia
4004 Wesbrook Mall Vancouver BC Canada V6T 2A3
[3]Department of Mechanical Engineering, University of British Columbia
2216 Main Mall Vancouver BC Canada V6T 1Z4
[4]The Pulp and Paper Centre, University of British Columbia
2385 Main Mall Vancouver BC Canada V6T 1Z4

## ABSTRACT

The mobility of sedimenting fibre suspensions is characterized here in three different, yet complementary studies. In the first study we present a simple mathematical analysis to define more precisely the term sediment concentration. Through this analysis we correct the sediment concentration for compressibility effects and redefine this parameter as the gel concentration point. In the second study, we visualize the transient settling of radioactively labeled papermaking fibres using a new experimental technique, positron emission tomography (PET). In the third study, we measure the mass distribution of fibres (formation) in the sediment as a function of the initial suspension concentration. The results indicate that the gel concentration point occurs at a crowding number of approximately 16(±4). Two distinct regimes of

settling were clearly identified with PET, depending upon the initial crowding number of the suspension ($N$). With $N < 16$, hindered settling was observed. With $N > 16$, fibres began to flocculate, starting with the long fibre fraction. Formation was found to be slightly dependent on $N$ in the region $N < 16$ and then worsen significantly with $N > 16$. In summary, these findings indicate that within the suspension conditions found in papermaking $1 < N < 60$, that there are two sub-regimes within these limits of differing levels of fibre mobility. These sub-regimes are delineated at $N = 16$.

## 1 INTRODUCTION

There is a need to characterize fibre suspensions in a simple manner that reflects its papermaking capability. A number of years ago, Wahren and his co-workers attempted this and developed a simple experimental approach to characterize the networking capabilities of the fibres by measuring the sedimentation concentration. While attractive because of its simplicity, this method has not been widely used, in part because of the difficulty to reproduce the experimental results, the uncertainties of what the measurement means to papermaking suspensions, and to some degree, to interpretation difficulties due to network compressibility. The objective of this study is to further explore the use of sedimentation to characterize papermaking fibre suspensions by addressing these earlier shortcomings.

Before summarizing the existing literature it is instructive to define the regimes of fibre interactions in the range used in papermaking, see for example the review of Kerekes et al [1]. Although fibre networks may occur by surface charges, Mason [2] found that mechanical entanglement rather than colloidal force was the principle source of fibre flocculation. Fibres collide because of the relative motion induced by the flow field. They entangle, bend, and remain networked from frictional forces transmitted by fibres that are locked into bent configurations [3]. Soszynski and Kerekes [4] confirmed the influence of bending stresses on floc strength through stress relaxation experiments. They defined the propensity for papermaking fibres to flocculate in terms of a dimensionless number, termed the crowding number $N$

$$N = \frac{C_m L_f^2}{2\omega} \tag{1}$$

where $C_m$ is the concentration of the solid material in the suspension having dimensions of kg $m^{-3}$; $L_f$ is an interaction length, with a dimension of m, based upon the length of a fibre ($l$); and $\omega$ is fibre coarseness defined as the mass per unit length of fibre, kg $m^{-1}$. It should be noted that for polydisperse suspensions Kerekes and Schell [5] recommend the use of the mean of the fibre length distribution $p(l_i)$ to estimate the interaction length, i.e

$$L_f = \sum p(l_i) l_i \tag{2}$$

The physical significance of $N$ is given by its definition; it reflects the number of fibres in a spherical volume of diameter equal to $L_f$. Flocculation does not generally occur when $N < 1$ as each fibre can rotate freely. The range of $1 < N < 60$ represents a regime of fibre behavior described by Soszynski [6] as one of 'forced collisions' between fibres in simple shear flow. It is in this range of $N$ that most papermaking operations occur, specifically in the range $10 < N < 45$. Three-point interfibre contact occurs at approximately $N \approx 60$. Fibres are locked into networks having mechanical strength at this point.

Understanding the motion of dilute ($N \ll 1$) fibre suspensions is difficult. Insight into this phenomena can be gained by first examining the simplest case of the motion of a single isolated fibre settling under Stokes' flow conditions, i.e. [7]

$$\boldsymbol{V}_{sed} = \frac{\Delta\rho d_f^2}{16\mu}[(\ln 2r + 0.193 + O(\ln 2r)^{-1})\,\boldsymbol{g} + (\ln 2r - 1.807 + O(\ln 2r)^{-1})\,(\boldsymbol{p}\cdot\boldsymbol{g})\,\boldsymbol{p}], \tag{3}$$

where $\Delta p$ is the difference in density between the fibre and the surrounding fluid; $r$ is the aspect ratio of the fibre defined by $l/d$ where $d$ is the diameter of the fibre; $\mu$ is the viscosity of the fluid; $\boldsymbol{g}$ is the acceleration due to gravity; and $\boldsymbol{p}$ is a unit vector that indicates fibre orientation. Unlike spheres, fibres can have significant motion perpendicular to gravity with a drift velocity strongly dependent upon its orientation. Ross and Klingenberg [8] considered this case for papermaking fibres by dropping one fibre at a time into a quiescent fluid to create sediment. Using techniques similar to those employed by Doi and Chen [9] in polymer dynamics, these authors modeled papermaking fibres as a chain of prolate spheroids connected through elastic ball and socket joints in order to account for flexibility effects.

With semi-dilute suspensions ($1 < N < 60$), this situation becomes more complex as each individual fibre moves under the influence of the long-range hydrodynamic disturbances of the other particles. During sedimentation,

these disturbances lead to inhomogeneous settling rates [10] and local floc formation. With monodisperse suspensions, the latter has been observed by Kumar and Ramarao [11], and confirmed Herzhaft et al [12] (called clumps by these authors), who report the existence of flocs for monodisperse glass fibres settling at low crowding numbers. Kumar and Ramarao also noted that, as the fibre concentration increased, the number of flocs increased and caused greater hindrance effects. With bidisperse suspensions, Davis [13] observed size segregation up to a critical concentration, above which particle interlocking prevented further segregation. It was found that the smaller the ratio of the large to small particle diameters, the smaller the critical concentration. Quite possibly due to these complexities, there are only a few mathematical models of the motion of interacting particles [7,14,15]. Koch and Shaqfeh [15] considered the sedimentation of stiff, axisymmetric, nonspherical particles in a dilute suspension and demonstrate that particle flocculation can occur. Moreover, from a stability analysis, they suggest that the sedimenting suspension should segregate into regions of high particle density and cause a relatively strong downward convection of particles.

With sedimenting concentrated suspensions ($N > 60$), many authors consider the network to behave like a compressible porous medium [16,17]. As a result, the transport of mass and momentum can be expressed by Eularian volume-averaged two-phase flow equations [18,19,20]

$$\frac{\partial \phi}{\partial t} + \nabla \cdot (\phi \boldsymbol{u}) = 0 \tag{4}$$

$$\frac{\partial [1-\phi]}{\partial t} + \nabla \cdot [(1-\phi)\boldsymbol{w}] = 0 \tag{5}$$

$$-\phi \nabla P - \nabla \cdot \bar{\tau} + \rho_f \phi \boldsymbol{g} - \boldsymbol{M} = 0 \tag{6}$$

$$-(1-\phi)\nabla P + \rho_w (1-\phi)\boldsymbol{g} + \boldsymbol{M} = 0 \tag{7}$$

where $\phi$ is the volume fraction of the fibres; $\boldsymbol{u}$ and $\boldsymbol{w}$ are the velocities of the fibres and the water, respectively; $P$ is the fluid pressure; $\boldsymbol{M}$ is the inter-phase momentum term; $\rho_f$ and $\rho_w$ are the densities of the fibre and water, respectively; and $\bar{\tau}$ represents the fibre-fibre contact stress tensor as the fibre phase is conceptually envisioned as a continuum [21]. The inter-phase momentum term can be expressed by a Darcy formulation [16,17].

$$\boldsymbol{M} = \mu \frac{(1-\phi)}{k(\phi)} (\boldsymbol{u} - \boldsymbol{w}) \tag{8}$$

where $k(\phi)$ is the permeability of the network and is regarded as empirical function which must be determined from experiment [16,17,22,23,24, 25,26,27,28]. Finally, a large body of literature is available which ascribes $\bar{\tau}$ as an implicit function of the local solidity of the network, i.e. $\bar{\tau} = f(\phi)\bar{I}$ [16,24,29], where $\bar{I}$ is the identity tensor. A number of authors have represented the functional relationship between $f$ and $\phi$ by power-law functions of the type [30,31,32]

$$f(\phi) = m(\phi^n - \phi_g^n) \tag{9}$$

$$f(\phi) = m(\phi - \phi_g)^n \tag{10}$$

where $\phi_g$ is the "gel" point and is defined as the value below which $f(\phi)$ cannot be distinguished from zero. This value has not been experimentally determined and is commonly assumed to be small in comparison to $\phi$. Here, $m$ and $n$ are empirical constants determined from static compressibility tests and are defined uniquely for each relationship given above. It should be noted that this formulation for $\bar{\tau}$ neglects shear stress that comes about from network deformation. It thereby assumes isotropic material behavior. These formulations also neglect plastic deformation and time-dependent behavior that has shown to be important.

In summary, the existing theoretical work regarding sedimentation of dilute and semi-dilute fibrous suspensions is limited as the process of mechanical entanglement has not been considered. Further, numerical studies with polydisperse suspensions have yet to be performed. Most previous experiments have been confined to the measurement of the settling velocity of the interface between the clear fluid and the suspension. With concentrated suspensions, we find that the equations of motion are not a closed system of equations. The success of a mathematical model in this case is dependent on the accuracy of the closure equations for inter-phase momentum transport and the fibre-fibre contact stress. These must be determined by experiment. None of these previous studies address the issue of employing sedimentation to characterize the mobility of fibres in papermaking suspensions. Our objective in this paper is to do so.

This paper is organized in three sections. In Section 2, we explore the transient settling process with a new tool, positron emission tomography (PET). Here, we study the transient behavior of Flourine-18 (F-18) labeled papermaking fibres settling by gravity in the midst of a suspension of unradioactive fibres using PET. We measure the concentration profile of the radioactive tracer along the sedimentation axis as a function of time. The experimental conditions were such that the particle Reynolds number was

always low and the crowding number was set between 10 and 53. This ensures that interfibre contact is significant in the suspensions. The key advantage of this measurement technique is its applicability to assess the mobility of several fibre classes within a papermaking fibre suspension. In Section 3, we present a mathematical analysis that allows a more rigorous interpretation of the sediment concentration by relating it to the gel concentration point. Finally, in Section 4, we link the flocculation tendency of papermaking suspensions, determined from formation measurements to the mobility of the individual fractions and the gel concentration point.

## 2 TRANSIENT SETTLING PROCESS

### 2.1 Background

There are a number of experimental techniques currently available to visualize the settling process: light transmission [33], X- or $\gamma$-ray attenuation [18,34], acoustics [35,36], or nuclear magnetic resonance [37,38,39,40]. For papermaking suspensions, it is important to measure both the velocity of the various fibre fractions within a suspension, from low to high crowding numbers, in order to gain insight into the bulk motion of the suspension. The experimental measurements mentioned above are "global" in nature in that the motion of individual particles cannot be detected. Herzhaft et al [12] have recently visualized the motion of marked fibres, in a suspension of unmarked fibres made optically transparent by matching the index-of-refraction. Although this technique worked well with glass fibres, where all particles have similar physical properties, this technique would be difficult to use with papermaking suspensions. As a result, the objective of this work is to develop a method to visualize the motion of the various fibre length fractions in papermaking fibre suspensions. We do so using a new tool: positron emission tomography (PET).

### 2.2 Experimental technique

#### *2.2.1 Suspensions*

A suspension of thermomechanical pulp fibres in water was used in this work. Fibre-length fractions of this suspension were obtained by classification in a Bauer-McNett Classifier. Fractions of various fibre lengths were collected separately and stored for further testing. Fibre length and coarseness were measured for each fraction with an automated fibre length analyzer (FQA). Three fibre fractions were chosen for further study. We will refer to

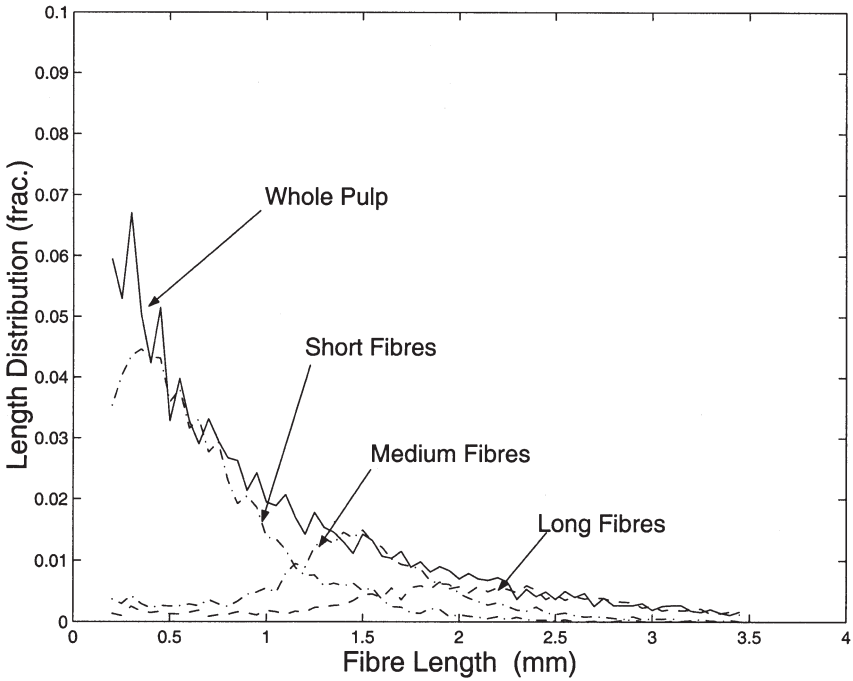


**Figure 1** The Fibre Length Distributions. The long fibres had an average length of 2.0(± 0.8) mm, the medium fibres had an average fibre length of 1.4(±0.6) mm and the short fibres had an average length of 0.7(±0.4) mm. The whole pulp suspension had an average fibre length of 1.0(±0.7) mm with $w = 0.19$ mg/m.

these as the "long" , "medium", and "short" fibre fractions in this study. The fibre length distributions of the fractions and of the whole pulp are shown in Figure 1. Based upon the initial settling velocities reported by Marton and Robie [41] for mechanical pulp fibres, we estimate the fibre Reynolds number, defined as $lV_s\rho_f/\mu$, to be approximately $10^{-2}$. Thus, the effect of inertial forces is assumed negligible for the experimental conditions tested.

The sedimentation experiments were performed in a plastic jar with a circular cross-section having an inner diameter of 87 ±1 mm and a height of approximately 145 ±3 mm. This represents a diameter which is at least 40$l$, based upon the long fibre fraction. This is sufficiently large to accurately measure bulk properties in the middle of the suspension as Russel et al [42] have demonstrated that the motion of a fibre is influenced by the wall over

distances smaller than about a six fibre lengths. It should be noted that the plastic jar was slightly rounded at the bottom with a radius of curvature measured to be 200 mm.

The settling experiments were conducted by first radioactively labeling a selected Bauer-McNett fraction of fibres with F-18 and reintroducing this into the original suspension. Details of the labeling procedure have been described previously [43]. Briefly, the fibres were suspended in a solution of acetic acid while 18F-$F_2$ was bubbled through the suspension at 10 ml/min with constant stirring. After the addition of the flourine the fibres were filtered and washed with distilled water. At this point the fibres were labeled with F-18 with a 10% yield based upon the total radioactivity introduced. F-18 has been chosen here in preference to other positron emitting tracers such as O-15, C-11, or N-13 because of its reasonably long half-life of 110 minutes and its reactivity with pulp fibres.[1] A known mass of both the radioactive tracer and non-radioactive fibres were added to the sedimentation jar and the rest of the jar was filled with water. Care was taken to recreate the same fibre length distribution for the whole pulp suspension. Typically, 0.3 g of radioactive fibres were used for each experiment. Air was removed from the suspension by using vacuum and the suspension was mixed by rotating and tumbling the jar for approximately 5 minutes. Three suspension concentrations were studied, namely 1.7, 5.0, and 9 kg $m^{-3}$ which represent initial crowding numbers of $N_o = 10$, 30, and 53, respectively. At the lower two suspension concentrations, four experiments were conducted to visualize the motion of the three individual fibre fractions and the whole pulp during settling. Only the short fibres and the whole pulp were visualized with the 9 kg $m^{-3}$ suspension. In total ten experiments were conducted.

### 2.2.2 *Visualization*

Positron emission tomography (PET) is an imaging technique widely developed for diagnostic medicine but has recently been applied to engineering studies [45,46,47,48,49,50,51,52]. Each emitted positron annihilates with a nearby electron producing two co-linear 511 keV $\gamma$-rays traveling in opposite directions. Simultaneous detection by position sensitive detectors located on either side of the system [53] defines a line close to which the radioactive decay must have occurred. By detecting many of these decays, the distribution of activity can be determined. With the tomograph used here (Siemens

[1]It should be noted that other radioisotopes have been used to label pulp fibres. These include I-131, Ba-140, Cu-64, Ce-140, I-194, and Au-198 [44]. These labeled fibres, however, have never been used in conjunction with PET.

ECAT 958B), images are scanned along 31 different parallel planes, 3.37 mm thick, to give an axial extent of approximately 100 mm. Each axial plane is made up of 128 × 128 pixels, 2.53 $mm^2$.

Two different imaging protocols were employed. With the 1.7 kg $m^{-3}$ suspension, a total of 67 images were captured over one hour of imaging. The framing rates were as such: 4 images at 15 second exposure times over the first one minute; 8 frames with 30 second exposures over the next 4 minutes; and then 55 images at one minute exposure times. With the higher concentration suspensions, a total of 25 images were taken over one hour of settling: 10 images at 30 second exposure times for the first five minutes; 5 images at 60 second exposures over the next five minutes; and then 10 images at 60 second exposures taken every 5 minutes. Using the initial settling velocities reported by Marton and Robie [41], we anticipate the sediment to move about 1/4 of a pixel over the longest exposure times used (one minute). After each experiment, a 'transmission scan' was made in order to calculate the corrections for photon attenuation from the settling jar and the non-radioactive materials in the suspension. The transmission scan was performed after the radioisotope was allowed to decay for approximately 10 half-lives.

### 2.3 Results and discussion

The transmission scan provided the necessary calibration for calculating the true activity so that the data can be reconstructed into 3D emission images as given in Figure 2. Activity was then related to the mass of radioactive fibres from an independent calibration procedure, see Figure 3. In most sedimentation studies found in the literature, researchers usually assume that the spatial distribution of particles in the horizontal plane is uniform. This assumption can be verified with these images and we estimate that the variation in each horizontal plane to be approximately 17%. This estimate remains essentially constant for every time step. As a result, we represent the dynamics of the sedimentation process as vertical concentration profiles determined from averages of square sub images (46 × 46 mm), sampled from the center of the sedimenting jar. Image reconstruction and analysis was performed with MATLAB.

It should be noted that we are uncertain of the concentration measurement in the first few pixels near the top of the sediment. There are two phenomena that need to be considered here. It is well known that at interfaces between radioactive and non-radioactive materials, PET-images appear somewhat "smeared" when reconstructed. Smearing generally occurs over 2–3 pixels. On the other hand, a naturally occurring concentration gradient must exist at

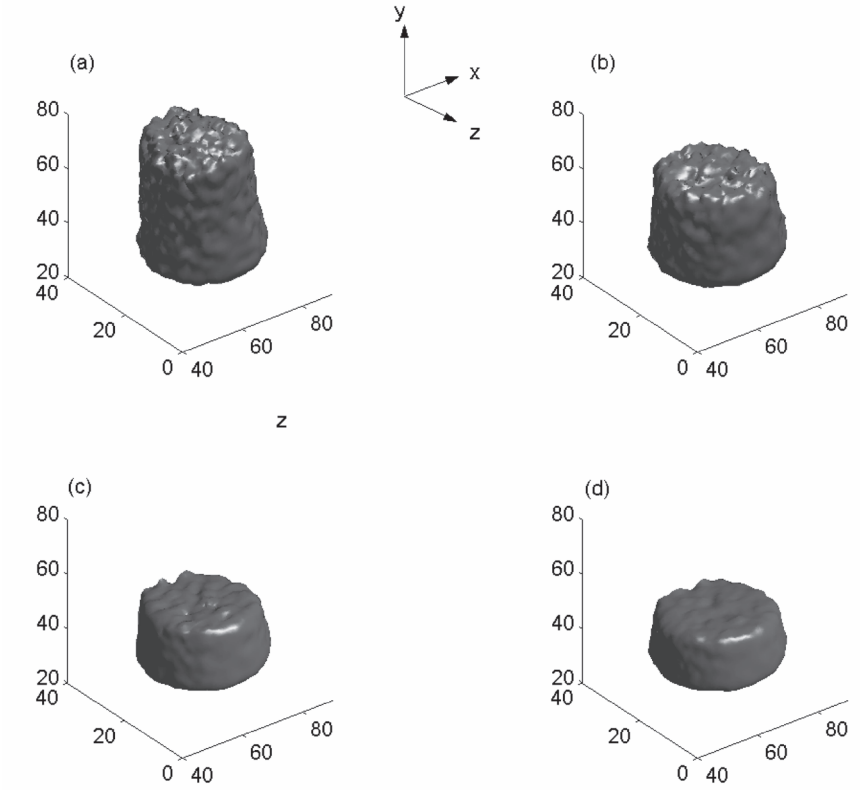


**Figure 2** A three-dimensional reconstruction of the radioactivity distributions inside the settling jar at different times: (a) t = 4, (b) t = 12, (c) t = 20, (d) t = 28 min. The axes represent the pixel positions.

this point due to polydispersity and hydrodynamic self-diffusion effects [37]. Accurately decoupling the "smearing" from the real concentration gradient is difficult, if not impossible. In this work we do not attempt to decouple these effects but instead, delineate the areas of uncertainty in the measured signal by the hatched lines given in Figure 4, see Appendix A for more details. In this Figure, the sedimentation axis has been normalized with respect to the initial height of the suspension. The decrease in the signal at approximately 5 mm from the bottom of the container reflects the fact the bottom of the jar was rounded. By integrating these curves, we find that the total radioactivity remained essentially constant for every time step. The total radioactivity was

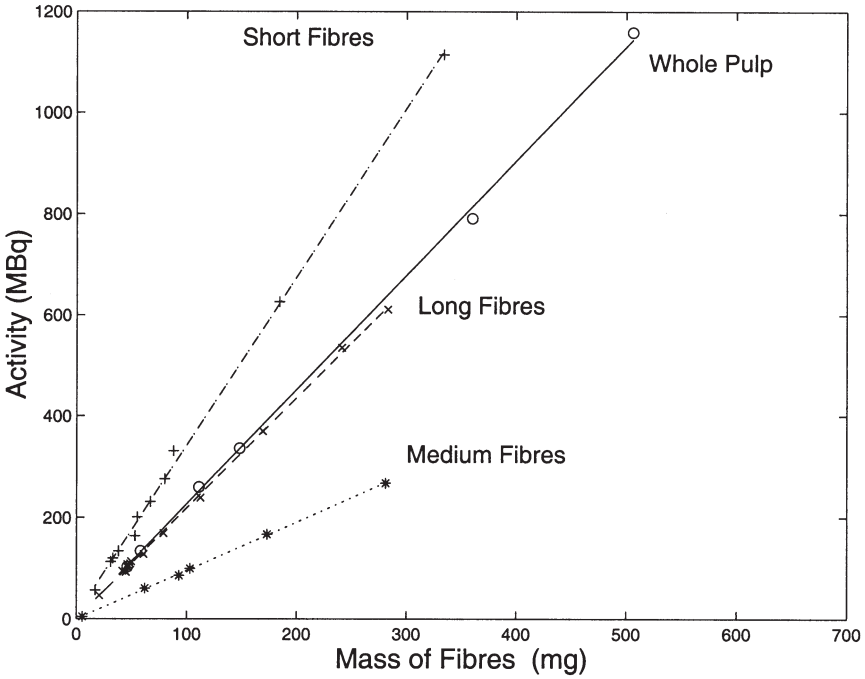


**Figure 3** The calibration curve between the mass of fibres labeled and the measured activity. The slopes of these curves were found to be 2.3(±0.1), 2.2(±0.1), 0.9(±0.1), and 3.5(±0.2) MBq/mg for the whole pulp, long, medium and short fibres, respectively.

found to vary by at most 4% and this demonstrates the internal consistency of the measurement technique.

The form of these profiles were found to be similar for all cases tested and the example shown clearly illustrates the dynamics of sedimentation process. We complement this result by reporting the height of the interface between the suspension and the clear water for all fibre fractions tested, as shown in Figure 5. We find that initially the interface moves downward at a constant rate as a layer of sediment builds up at the bottom of the container. We speculate that as the interface approaches the height of sediment, its rate of fall decreases until a "critical settling point" is reached when a direct interface is formed between the sediment and the non-radioactive material. At this point the sedimentation rate decreases dramatically. We estimate from this

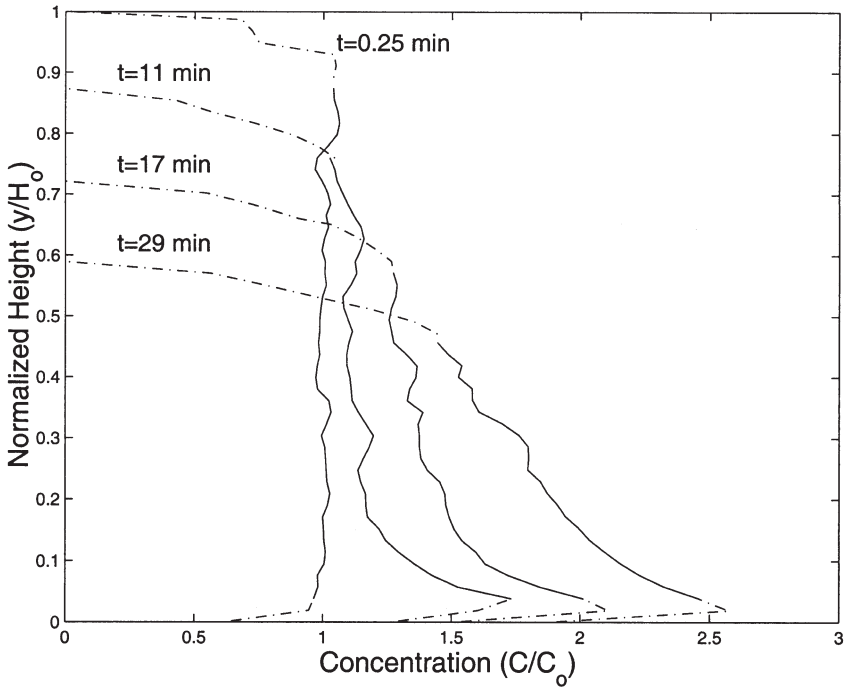


**Figure 4** PET measured concentration profiles with the "whole" pulp fraction made radioactive. The initial crowding number of the suspension was 10. The bottom of the jar is located at $y = 0$.

figure that the critical settling point occurs at $t = 12$ minutes which represents an overall crowding number for the suspension of $N_{critical} \approx 16$. The significance of this finding will be discussed in Section 3. Further sedimentation beyond this point results solely from the consolidation of the sediment. Finally, it is interesting to note in Figure 4 that at $t = 29$ minutes a large concentration gradient is evident in the sediment.[1] The porosity of the sediment is smallest at the bottom because the compressive force due to the weight of the fibres is greatest. Although network compressibility has been observed by other researchers [16,17,22], Figure 4 illustrates that it leads to a

[1]We must also note that we have not reached steady state after one-hour of sampling. Through optical measurements, steady state was achieved when $h_s/H_o = 0.26$.

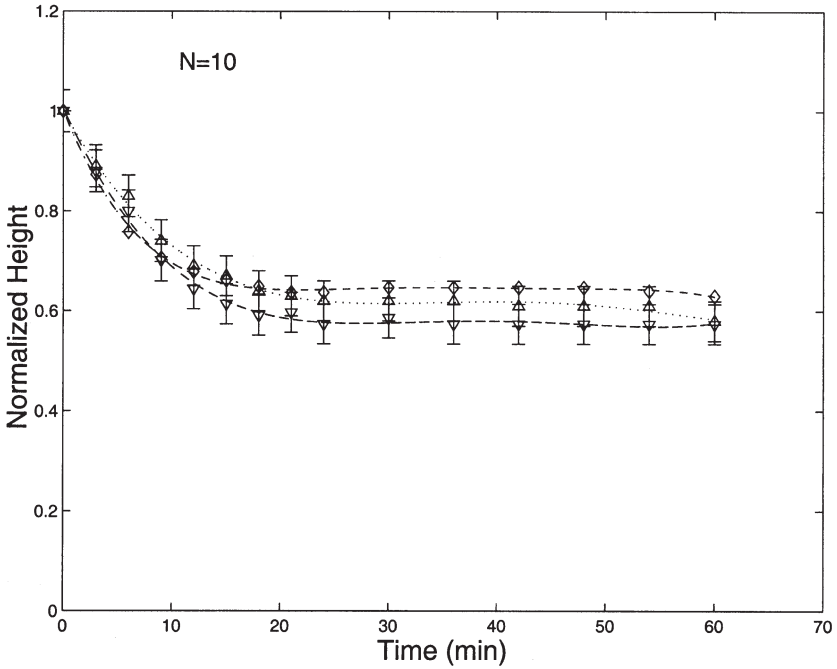


**Figure 5** The movement of the interface between the radioactive tracers and the clear fluid measured as a function of time. Each tracer is differentiated by the type of symbol used (▽ long fibres, ◊ medium fibres, or △ short fibres). The uncertainty in the measured height of the interface is given by the error bars.

very significant concentration gradient in the sediment to a degree that the use of an average sediment concentration is questionable as a means of characterizing the suspension.

With the uncertainty in the measured interfacial heights, we found no statistical difference between the settling rates of the different fibre fractions in the region when $t < 12$ min, see Figure 5. This contrasts the results of Marton and Robie [41] who report that long fibres settle at higher rates than shorter ones, when tested separately, i.e. when the individual fibre fractions are allowed to settle by themselves. Our findings apply to settling rates of fibre fractions inside in a mixture. This phenomena results from the fact that larger fibres are retarded to a greater extent than the smaller ones in these concentration regimes.

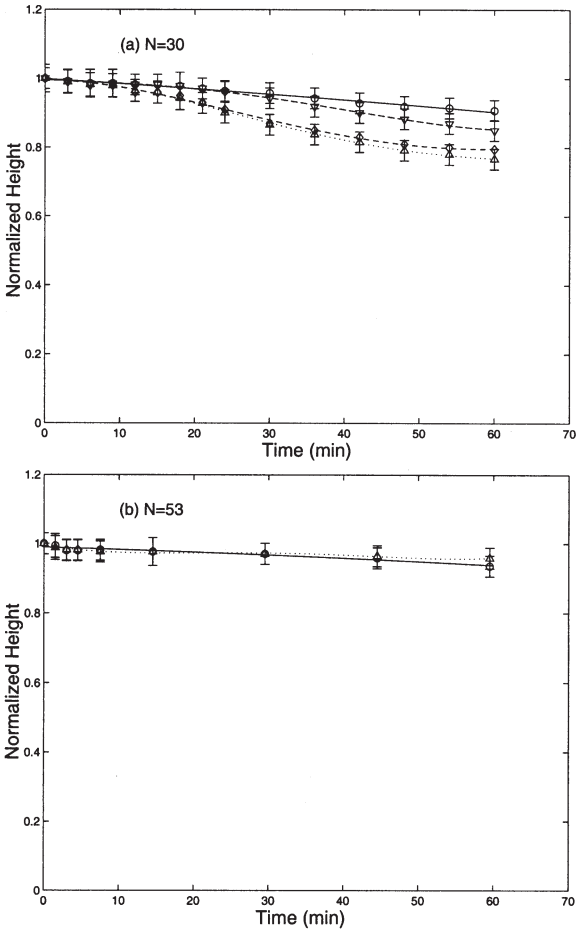


**Figure 6** The descent of the radioactive interface for all of the experiments conducted. Each tracer is differentiated by the type of symbol used (○ whole pulp, ▽ long fibres, ◊ medium fibres, or △ short fibres). The uncertainty in the measured height of the interface is given by the error bars.

The sedimentation curves for the higher concentration suspensions are shown in Figure 6. At $N = 30$, we see that the short and medium length fibre fractions settle at a higher rate than the long fibre fraction, and that the long fibres settle at approximately the same rate as the whole pulp suspension. This

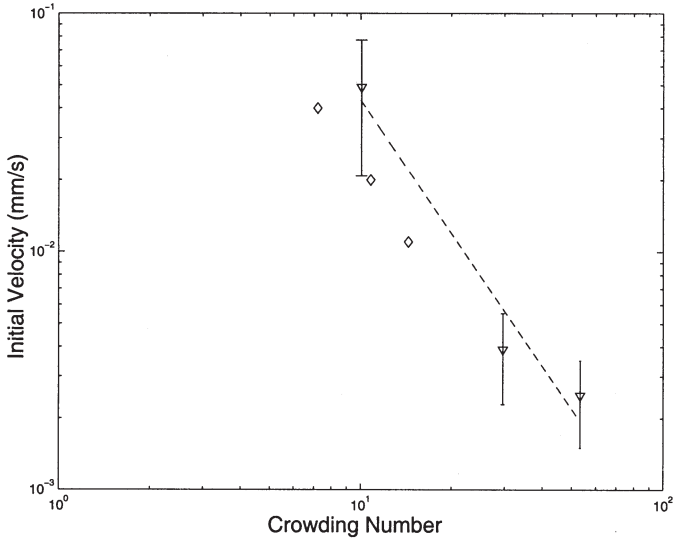


**Figure 7** The initial sedimentation rates for whole pulp suspensions determined from the slope at $t = 0$ of the interface height versus time curves. Initial velocities measured from PET are shown as ▽. The data from Marton and Robie are shown as ◊.

occurs because long fibres have greater contact with other fibres than do short and medium length fibres. At $N = 53$, the short fibres and the whole pulp suspension settle at approximately the same rate. This suggests that a continuous network is formed in this range. We suggest that network formation commences with immobilization of the long fibres, while the shorter fibres are still mobile, and continues until all fibre fractions are immobile.

Finally, we can compare the initial settling velocities of the whole pulp suspensions with data found in the literature, see Figure 7. Clearly, our results are similar to those reported by Marton and Robie [41]. The data from Marton and Robie [41] were measured on mechanical pulp fibres with an estimated length of 1.2 mm and coarseness of 0.2 mg/m (pulp code 30).[1] This closely approximates the physical properties of the fibres used in this study and confirms the utility of this approach.

[1]The coarseness and length used from this study are averages of the reported fractions. The length and coarseness of the whole pulp was not given in this report.

## 3 GEL CONCENTRATION POINT

### 3.1 Background

In the previous section, we established the usefulness of PET to characterize fibre mobility in a settling suspension. We also showed that significant concentration gradients existed over the depth of the sediment implying that there is no unique sediment concentration. While this gradient can be minimized with very small sediment depths, significant inaccuracies may arise in the measurement of these depths. To make sediment tests a useful means of characterizing fibre suspensions, these shortcomings must be overcome. We do so here by developing a method which accounts for compressibility effects.

At steady-state, the particle network stress gradient in the settled sediment must balance the gravitational field throughout its depth. The balance of forces[1] on a volume element of the sediment and an overall mass balance are given by

$$\frac{\partial f(\phi)}{\partial y} = -\Delta\rho g\phi \tag{11}$$

$$\phi_o H_o = \int_0^{h_s} \phi dy \tag{12}$$

where $\phi_o$ is the original solidity of the suspension, defined by $\phi_o = C_o/\rho_f$; $H_o$ is the initial height of the sediment; and $h_s$ is the sediment height. The required boundary condition is that $f(\phi) = 0$ at $y = h_s$. The form of the solution depends upon the functional relationship for $f(\phi)$ (cf. Equations 9 and 10). We proceed to solve these equations for each formulation. The solution using Equation 9 is presented here, while the solution with Equation 10, which proceeds along similar lines, is presented in Appendix C. Both formulations give the same result.

We begin by substituting Equation 9 into Equation 11, that is

$$\phi^{n-2}\,\frac{\partial\phi}{\partial y} = \frac{-\Delta\rho g}{mn}, \tag{13}$$

which gives

$$\phi(y) = \left[\frac{\Delta\rho g(n-1)}{mn}(h_s - y) + \phi_g^{n-1}\right]^{\frac{1}{n-1}} \tag{14}$$

when integrated. With this, Equation 12 can be solved to give

[1]This is derived from Equations 6 and 7 and is shown in Appendix B.

$$\phi_o = \frac{m}{\Delta\rho g H_o}\left[\left(\phi_g^{n-1} + \frac{\Delta\rho g(n-1)}{mn} h_s\right)^{\frac{n}{n-1}} + \phi_g^{\,n}\right]. \tag{15}$$

This relationship states that their is a unique functional relationship between the final sediment height $h_s$ and the initial solidity of the suspension $\phi_o$, for a given set of experimental conditions. This can easily be measured in the laboratory. By doing so, we can estimate the gel concentration from the initial slope of this relationship, i.e.

$$\lim_{h_s \to 0}\left(\frac{d\phi_o}{dh_s}\right) = \frac{1}{H_o}\lim_{h_s \to 0}\left[\phi_g^{n-1} + \frac{\Delta\rho g(n-1)}{mn} h_s\right]^{1/(n-1)} = \frac{\phi_g}{H_o} \tag{16}$$

### 3.2 Experimental technique

The sediment concentration was measured in a smaller glass-walled cell of circular cross-section with an inside diameter of 55 mm and a height of 35 cm. The sediment concentration was determined using a simple procedure. First a known mass of oven-dried fibres were soaked in water, dewatered in a Buchner funnel, and then diluted to a known concentration ($C_o$). The suspension was then agitated and allowed to settle in the sediment jar. After twenty-four hours the pad height was determined from graduations marked onto the side of the cylinder. This procedure was repeated at different initial suspension concentrations and the ratio of sediment height ($h_s$) to initial height $H_o$ was recorded as a function of $C_o$, see Figure 8. The initial height was held constant from test to test and set to be $H = 25$ cm. Fibre length and coarseness were determined after each experiment using an automated fibre length analyzer (FQA). The gel point was estimated from the slope of the curve at $h_s/H_o \to 0$.

### 3.3 Results and discussion

The gel concentration was determined for twenty different fibre suspensions having a wide range of fibre length and coarseness and the results are shown in Figure 9. Of particular interest is the effect of fibre length and coarseness. These are the two major properties of pulp fibres and they both play a role in the crowding number. In Figure 9, the gel concentration is related to the ratio of coarseness and interaction length squared. The independent variable was chosen in this case with respect to the form of Equation 2, that is the slope of this curve is proportional to the crowding number. In general terms, $\omega/L_f^2$ was small for suspensions with a large fraction of softwood fibres. With the

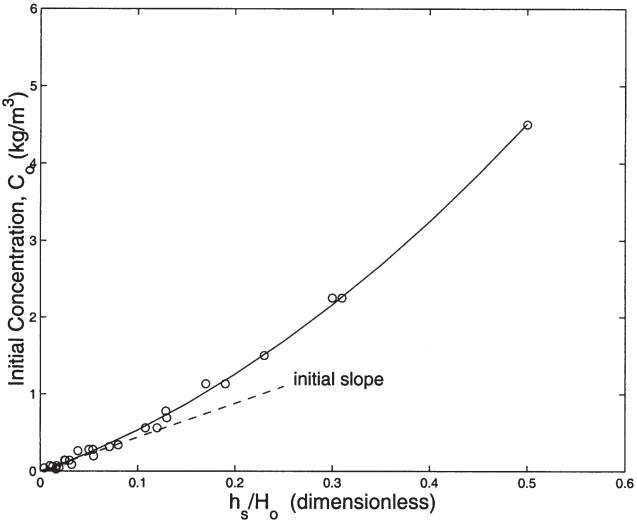


**Figure 8** The height of the sediment recorded as a function of initial suspension concentration. The initial slope of the curve is used as an estimate of the gel concentration. A pure aspen fibre suspension was used in this example with a length-weighted fibre length average of 0.88 mm and a coarseness of 0.10 mg/m.

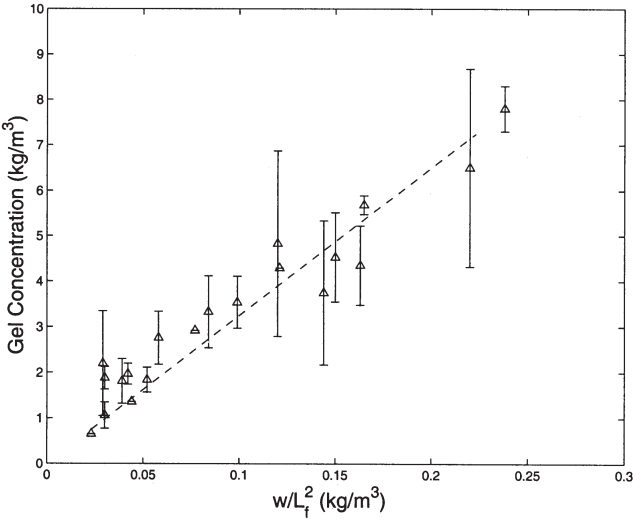


**Figure 9** The gel concentration point for a number of different hardwood and softwood suspensions as determined by the method outlined in Section 3.

error associated with the data, we see that the gel concentration point increased nearly linearly with increasing $\omega/L_f^2$. The correlation coefficient was determined to be $r^2 = 0.9$. A higher order function was not justified for this case as there are large uncertainties associated wth the measurement. The linearity found in Figure 9 implies that the gel concentration point occurs at a constant crowding number of $N = 16 \pm 4$. This crowding number is the same as the critical crowding number defined in Section 2.3.

At this point it is instructive to reiterate the definition of the gel concentration point. It is the lowest concentration at which the network can support load. To do so, the interfibre contacts must be sufficiently large to create a "backbone" which spans the entire suspension. This concept can be illustrated from the sedimentation curve shown in Figure 5. In this case settling started with $N_o < N_{critical}$ and proceeded at a relatively fast rate until the average suspension crowding number was $N \approx 16$. We postulate that at this condition a continuous fibre network formed which 'bridged' the entire sediment. This increased the resistance to relative fibre motion resulting in a dramatic decrease in the settling rate. Hence, network formation hinders the sedimentation rate. We postulate that the gel concentration point represents the suspension concentration at which the level of interfibre contact is such that a network can bear load.

## 4 FIBRE MASS DISTRIBUTION (FORMATION) OF THE SEDIMENTS

### 4.1 Background

In the previous sections, we showed by PET and a simple settling test that a gel concentration point existed for fibre suspensions. The gel concentration was found to occur at a critical crowding number of $N_{critical} = 16$ for all fibre suspensions tested. At this point, a continuous network is formed in the suspension. From these findings, we postulate that $N_{critical}$ has importance in characterizing the mobility of fibre suspensions, and thereby the uniformity of fibre distribution (formation) of paper. The objective of this part of the work is to examine whether this is the case.

### 4.2 Experimental technique

The variation of the mass distribution (formation) of the sediment was measured using a simple procedure. Handsheets were made from three different fibre suspensions having a wide range in length and coarseness. We will refer to these as "fibre type 1" ($\omega = 0.24$ mg/m, $L_f = 2.15$ mm), "fibre type 2"

($\omega = 0.15$ mg/m, $L_f = 0.87$ mm), and "fibre type 3" ($\omega = 0.13$ mg/m, $L_f = 2.3$ mm) in this study. Paper samples were made using typically 1.2 g of fibres in a standard British sheet former to produce sheets with a grammage of 60 g $m^{-2}$. The initial crowding number for each test was altered by diluting each suspension with various amounts of water. During each test, the fibres were dispersed by agitation and allowed to settle. The sediment was carefully removed from the apparatus and then pressed and dried using the TAPPI standard methods. Formation was measured using an Ambertec $\beta$-formation tester. In this method, grammage of 400 circular zones having a diameter of 1 mm is measured and the standard deviation of the grammage $\sigma$ is calculated.

## 4.3 Results and discussion

### *4.3.1 Dimensional analysis*

Without chemical additions, fillers, or hydrodynamic shear, $\sigma$ depends primarily upon five parameters – initial consistency $C_o$, coarseness $\omega$, length-weighted fibre length average $L_f$, basis weight $B$, and size of the inspection zone x. We may derive a relationship between $\sigma$ and these five parameters from the general form

$$\sigma = f(C_o, \omega, L_f, B, x) \tag{17}$$

by dimensional analysis. To do so we consider the units of each parameter, using the brackets [ ] below to mean "has the units of":

$$\sigma = \left[\frac{kg}{m^2}\right] \tag{18}$$

$$C_o = \left[\frac{kg}{m^3}\right] \tag{19}$$

$$\omega = \left[\frac{kg}{m}\right] \tag{20}$$

$$L_f = [m] \tag{21}$$

$$B = \left[\frac{kg}{m^2}\right] \tag{22}$$

$$x = [m] \tag{23}$$

This indicates that the primary dimensions in this case are mass and length. If

we represent these dimensions by the mass and length of a fibre, i.e. ($\omega L_f$) and $L_f$, respectively, we may combine these variables with the remaining parameters into dimensionless groups. One such combination gives

$$\left(\frac{\sigma L_f}{\omega}\right) = f\left(N, \frac{BL_f}{\omega}, x^*\right) \tag{24}$$

where $x^*$ is defined by $x/L_f$. In this expression, $B$ is normalized to the fibre length and coarseness in the form $BL_f/\omega$. This dimensionless group has physical significance which we shall examine. ($BL_f$)/$\omega$ is in essence an "areal crowding number" ($n_a$) . This is defined as the number of fibres within a square area defined by the length of a single fibre, i.e.

$$n_a = \frac{B}{(\omega L_f)} L^2 = \frac{BL_f}{\omega} \tag{25}$$

If we assume a power-law relationship, we may express Equation 24 as

$$\left(\frac{\sigma L_f}{\omega}\right) = a(x^*)^b (N)^c (n_a)^d \tag{26}$$

where $a$, $b$, $c$, and $d$ are empirical constants. Finally, formation is commonly defined in the literature as specific formation ($\sigma/\sqrt{B}$). This can be obtained from Equation 26 by setting $d$ = 1/2. This gives a new dimensionless grouping II which is expressed as[1]

[1]At this point it is instructive to review the work of Corte and Dodson [54] in order to gain insight into the functional form of Equation 26. Corte and Dodson have shown that for square inspection zones of length $x$, the variance of local grammage for a random distribution of fibres is given by

$$\sigma^2 = \frac{\omega L_f}{x^2} BK \tag{27}$$

where $K$ is a function of fibre geometry and the inspection size. We anticipate that Equation 29 and 27 are equivalent at very dilute conditions. Since $x = L_f x^*$ it follows directly that

$$\Pi = \frac{\sigma}{\sqrt{B}} \sqrt{\frac{L_f}{\omega}} = \frac{\sqrt{K(x^*)}}{x^*} \tag{28}$$

Hence Π can also be found in the Corte Dodson relationship.

$$\Pi = \frac{\sigma}{\sqrt{B}} \sqrt{\frac{L_f}{\omega}} = a(x^*)^b (N)^c \tag{29}$$

The formation of the different sediments are shown in Figure 10; Π versus $N$ is shown in this Figure for each individual fibre type ($x^*$ is constant for each fibre type). The first observation that can be made here is that two distinct regions are evident. With $N_o < 16$, we find that II increased somewhat with initial suspension crowding number. Since we determined by PET that the sedimentation rate of all fibre fractions was found to be essentially equal in this regime, we postulate that fibre mobility allows for local self-healing. With $N_o > 16$, formation worsened significantly with crowding number as the fraction of fibres mobile in the network decreased.

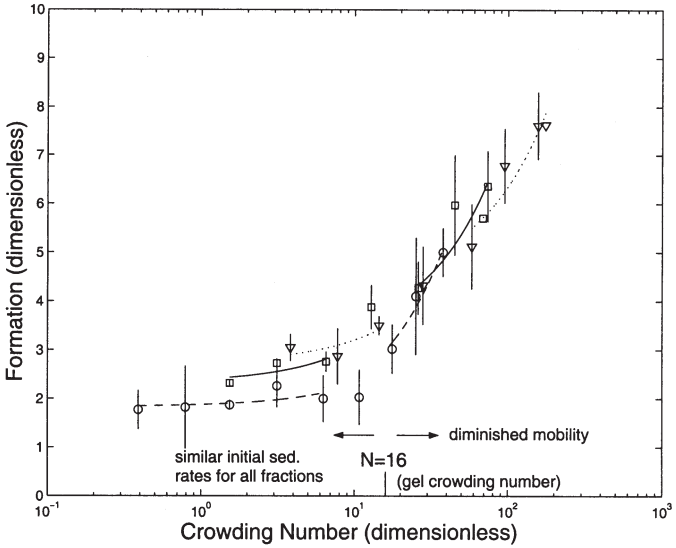


**Figure 10** The variation of the mass distribution of sediments formed at different crowding numbers (Note: the $x$-axis is logarithmic). The point $N = 16$ is also drawn in this Figure. Each fibre type is differentiated by the type of symbol used (□ = fibre type 1, 0 = fibre type 2, ▽ = fibre type 3). The uncertainty in the measured formation is approximately 15% which was determined through replicate testing. The lines in this figure were not determined by a regression analysis. They are included in this figure to aid in distinguishing the differences between the three fibre types The solid line corresponds to fibre type l. The dashed line to fibre type 2 and the dotted line to fibre type 3.

### *4.3.2 Limitations*

In this study we measured formation with an inspection area of 1 $mm^2$. It must be pointed out that the form of the curve is dependent upon the measurement technique.[1] Hence, any improvements in formation at scales smaller than this is below the detection limit of our method. The key finding here is that there is a change in the slope centered around the gel crowding number. We postulate that this change results from decreased fibre mobility of the long fibre fraction.

We must also state that this critical crowding number was determined at low Reynolds numbers, with no applied hydrodynamic shear, and in the absence of chemical deflocculants. These effects, we believe, would tend to increase the critical crowding number.

## 5 SUMMARY AND CONCLUSIONS

In this paper we characterized the mobility of papermaking suspensions though sedimentation in three different, yet complimentary studies. In the first study, we explored the transient settling process of papermaking fibres with a new tool, positron emission tomography (PET). Here, the motion of Flourine-18 labeled papermaking fibres were visualized settling in the midst of a suspension of non-radioactive fibres. The experimental conditions were such that the particle Reynolds number was always low and the initial crowding number of the suspension was set between 10 and 53, the levels found in typical headboxes. This ensured that fibre flocculation is one of the dominant components determining the behavior of the system. The key advantage of this measurement technique is that the mobility of the individual fibre fractions within a suspension can be determined. With this we identified two distinct regimes of settling, depending upon the initial crowding number of the suspension. With $N < 16$, hindered settling was observed. With $N > 16$, fibres began to flocculate, starting with the long fibre fraction.

In the second study, we defined more precisely the term sediment concentration based upon a mathematical analysis. Through this analysis we corrected the sediment concentration for compressibility effects and redefined this parameter as the gel concentration point. The gel concentration point represents the suspension concentration where a sufficient number of the fibres have flocculated to form a load-bearing network. This represents one

[1]This argument was brought forth by Prof. B. Norman, Dept. Paper Technology, KTH 2000, through email correspondence.

limit in fibre mobility. We determined the gel concentration point for 20 different pulp suspensions, having a wide range in fibre length and coarseness, and found this point to occur at a unique crowding number, $N = 16$.

From these findings we postulated that $N = 16$ has importance in ascertaining the mobility of fibre fractions in a suspension, and is thereby linked to the formation of paper through the self-healing effect. As a result, in the third study, we measured formation of hand sheets as a function of the initial crowding number of the suspension. Hand sheets were made by recovering the sediments after a settling experiment. In total, 90 hand sheets were tested made from 3 different fibre furnishes.

Here, we report formation in terms of a dimensionless group defined using a Buckingham-Pi analysis. If we represent the primary fibre variables of fibre mass and length by $(\omega L_f)$ and $L_f$, respectively, we obtain

$$\Pi = \frac{\sigma}{\sqrt{B}} \sqrt{\frac{L_f}{\omega}} == a(x^*)^b(N)^c \tag{30}$$

At large values of this dimensionless group, the formed sediment appeared grainy. π was found to be slightly dependent on $N$ in the region $N < 16$ as fibre mobility allowed for self-healing. π increased significantly in the region $N > 16$ as fibre mobility decreased.

Finally, the range of $1 < N < 60$ is of key importance to papermaking. Standard hand sheet making is carried out at a consistency which corresponds to $N \approx 1$ for softwood fibres. The aim in this test is to allow free movement of the fibres during draining. Three point interfibre contact occurs at approximately $N \approx 60$. The consistency of head box stock is generally set in the range of $10 < N < 45$. The aim here is to have the highest practical consistency that avoids network formation. These findings indicate that within the suspension conditions found in papermaking $1 < N < 60$, that there are two sub-regimes within these limits of differing levels of fibre mobility. These sub-regimes are delineated at $N = 16$. This value is at the lower end of the range used in commercial papermaking. This means headbox consistency may be optimized to a degree hitherto not done. However, whether this is possible on commercial machines remains to be proven. This requires further tests under more realistic forming conditions.

## ACKNOWLEDGEMENTS

The authors wish to thank Dr. Vesna Sossi for her help in the reconstruction and interpretation of the imaging results. We gratefully acknowledge financial support of TRIUMF through its Life Sciences program and from Forest Renewal BC through the Advanced Papermaking Initiative.

## REFERENCES

1. Kerekes, R.J., Soszysnki, R.M. and Tam Doo, P.A., "The flocculation of pulp fibres", *Fund. Res. Symp.*, Oxford (**1**): 265–310 (1985).
2. Mason, S.G., "Fibre motions and flocculation", *Pulp Pap. Mag. Can.,* **55**(13): 96–102 (1954).
3. Meyer, R. and Wahren, D., "On the elastic properties of three-dimensional networks", *Svensk Papperstid.*, **67**(10): 432–436 (1964).
4. Soszysnki, R.M. and Kerekes, R.J., "Elastic interlocking of nylon fibres suspended in liquid. part 2. process of interlocking", *Nordic Pulp Pap. Res. J.*, **3**(4): 180–184 (1988).
5. Kerekes, R.J. and Schell, C.J. "Effects of fibre length and coarseness on pulp flocculation", *Tappi J.*, **78**(2): 133–139 (1995).
6. Soszynski, R.M., *Fibre Flocculation in Shear Flow.* PhD thesis, University of British Columbia, Vancouver, BC, Canada, 1988.
7. Mackaplow, M.B. and Shaqfeh, E.S.G., "A numerical study of the sedimentation of fibre suspensions", *J. Fluid Mech*, **3766**: 149–182 (1998).
8. Ross, R.F. and Klingenberg, D.J., "Simulation of flowing wood fibre suspensions", *J. Pulp Pap. Sci*, **24**(12): 388–392 (1998).
9. Doi, M. and Chen, D., "Simulation of aggregating colloids in shear flow", *J. Chem. Phys.*, **90**: 5271–5279 (1989).
10. Turney, M.A., Cheung, M.K., McCarthy, M.J. and Powell, R.L., "Hindered settling of rod-like particles measured with magnetic resonance imaging", *IAChE J.*, **41**: 251–257 (1995).
11. Kumar, P. and Ramarao, B.V., "Enhancement of the sedimentation rates of fibrous suspensions", *Chem. Engng. Comm.*, **108**: 381–401 (1991).
12. Herzhaft, B., Guazzelli, E., Mackaplow, M.B. and Shaqfeh. E.S.G., "Experimental investigation of the sedimentation of a dilute fibre suspension", *Phys. Rew. Lett.*, **77**(2): 290–293 (1999).
13. Davis, R., "The experimental study of the differential settling of particles in suspension at high concentration", *Powder Technol*, **2**: 43 (1968).
14. Claeys, I.L. and Brady, J.F., "Suspensions of prolate spheroids in stokes flow. part 3. hydrodynamic transport properties of crystalline dispersions", *J. Fluid Mech*, **251**: 479–500 (1993).
15. Koch, D.L. and Shaqfeh, J., "The instability of a dispersion of sedimenting spheroids", *J. Fluid Mech*, **209**: 521–542 (1989).

16. Ingmanson, W.L. Andrews, B.D. and Johnson, R.C., "Internal pressure distributions in compressible mats under fluid stress", *Tappi J.*, **42**(10): 840–849 (1959).
17. Meyer, H., "A filtration theory for compressible fibrous beds formed from dilute suspensions", *Tappi J.*, **45**(4): 296–310 (1962).
18. Auzerais, F.M., Jackson, R., Russel, W.B. and Murphy, W.F., "The transient settling of stable and flocculated suspensions", *J. Fluid Mech.*, **221**: 613 (1990).
19. Yström, J., "On the Numerical Modeling of Concentrated Suspensions and of Viscoelastic Fluids". PhD thesis, Royal Institute of Technology (KTH) , Stockholm, Sweden, 1996.
20. Enwald, H., Peirano, E. and Almstedt, A.E., "Eulerian two-phase flow theory applied to fluidization", *Int. J. Multiphase Flow*, **22**: 21–66 (1996).
21. Tosun, I., Willis, M.S., Desai, F. and Chase, G.G., "Analysis of drag and particulate stress in porous media flows", *Chem. Eng. Sci.*, **50**(12): 1961–1965 (1995).
22. Robertson, A.A. and Mason, S.G., "Specific surface of cellulose fibres by the liquid permeability method", *Pulp Pap. Mag. Can.*, **12**: 103–110 (1949).
23. Nilsson, P. and Larsson, K.O., "Paper web performance in a press nip", *Pulp Pap. Mag. Can.*, **12**: T438–T445 (1968).
24. Han, S.T., "Compressibility and permeability of fibre mats", *Pulp Pap. Mag. Can.*, **5**: T134–T146 (1969).
25. Ellis, E.R., "Compressibility and Permeability of Never Dried Bleached Softwood Kraft Pulp and Its Application to the Prediction of Wet Pressing Behaviour", PhD Thesis, University of Maine, Orono, Me, USA, 1981.
26. Carlsson, G. and Lindström, T., "Permeability to water of compressed pulp fibre mats", *Svensk Paperstidning*, **86**(12): 128–134 (1983).
27. Ljungkvist, G., "Pulp Characterization by Permeability Measurement", PhD thesis, Chalmers University of Technology, Gothenburg, Sweden, 1983.
28. Vomhoff, H., "Dynamic Compressibility of Water Saturated Networks and Influence of Local Stress Variations in Wet Pressing", PhD thesis, Royal Institute of Technology, Stockholm, Sweden, 1998.
29. Wrist, P.E., "The present state of our knowledge on the fundamentals of wet pressing", *Pulp Pap. Mag. Can.*, **65**(7): T284–T296 (1964).
30. Wilder, H.D., "The compression and creep properties of wet pulp mats", *Tappi J.* , **43**(8): 715 (1960).
31. Ingmanson, W.L. and Whitney, R.P., "The filtration resistance of pulp slurries", *Tappi J.*, **37**(11): 523–534 (1954).
32. Jönsson, K.A-S. and Jönsson, B.T.L., "Fluid flow in conipressible porous media i: Steady state conditions", *AIChE J.*, **38**(9): 1340–1348 (1992).
33. Davis, R.H. and Birdsell, K.H., "Hindered settling of semi-dilute monodisperse and polydisperse suspensions", *AIChE J.*, **34**: 123 (1988).
34. Bergström, L., "Sedimentation of flocculated alumina suspensions: γ-ray measurements and comparison with model predictions", *J. Chem. Soc. Faraday Trans*, **88**(21): 3201–3211 (1992).
35. Bacri, J.-C., Hoyos, M. Rakotomalala, N., Salin, D., Bourlion, M., Daccord, G., Lenormand, R. and Soucemarianadin. S., "Ultrasonic diagnostic in porous media and suspensions", *J. Phys. III*, **1**: 1455–1466 (1991).

36. Martin, J., Rakotomalala, N. and Salin, D., "Accurate determination of the sedimentation flux of concentrated suspensions", *Phys. Fluid*, **7**(10): 510–911 (1995).
37. Turney, M.A., Cheung, M.K., McCarthy, M.J. and Powell, R.L., "Magnetic resonance imaging study of sedimenting suspensions of noncolloidal spheres", *Phys. Fluid*, **7**(5): 904–911 (1995).
38. Bobroff, S. and Phillips, R.J., "Nuclear magnetic imaging investigation of sedimentation of concentrated suspensions in non-Newtonian fluids", *Phys. Fluids A*, **42**(6): 1419–1436 (1992).
39. Lee, S., Jang, Y., Choi, C. and Lee, T., "Sedimentation of noncolloidal bidisperse suspensions", *Phys. Fluids A*, **4**(12): 2601–2605 (1992).
40. Cheung, M.K., Powell, R.L. and McCarthy, M.J., "Sedimentation of noncolloidal bidisperse suspensions", *AIChE J.*, **42**(1): 271–276 (1996).
41. Marton, R. and Robie, J.D., "Characterization of mechanical pulps by a settling technique", *TAPPI J.*, **22**(12): 2400–2406 (1969).
42. Russel, R.J., "Study of the sedimentation of noncollodial bidisperse suspensions by an acoustic technique", *J. Fluid Mech.*, **6**: 3809–3817, 177.
43. Jivan, S., Martinez, D.M., Buckley, K., Lindström, A., Olson, J.A., Adam, M.J. and Ruth, T.J., "The synthesis of f-18 labeled pulp fibres for pep", *Submitted to Appl. Radiat. Isotopes* (2000).
44. Moreira, R.M. and Felder, R.M., "Residence time distributions of pulp and paper slurries in vertical laminar flow", *AIChE J.*, **25**(1): 131–143 (1979).
45. Bridgewater, J., Broadbent, C.J. and Parker, D.J., "Study of the influence of blade speed on the performance of a powder mixer using positron emission tomography", *Trans IChemE*, **71**: 675–681 (1993).
46. Broadbent, C.J., Bridgewater, J., Parker, S.T., Keningley, D.J. and Knight, P., "A phenomenological study of a batch mixer using a positron camera", *Powder Technol.*, **76**: 317–329 (1993).
47. Broadbent, C.J., Bridgewater, J. and Parker, D.J., "The effect of fill level on powder mixer using a positron camera. *Chem. Eng. J. Bioch Eng.*, **56**(3): 119–125 (1995).
48. GarNcarek, Z., Przybylski, L., Botterill, J.S.M., Broadbent, C.J. and Bridgewater, J., "A measure of the degree of inhomogeneity in a distribution and its application in characterising the particle circulation in a fluidized bed", *Powder Technol.*, **80**: 221–225 (1994).
49. Sneiders, F.F., Hoffmann, A.C., Cheesman, D., Yates, J.G., Stein, M. and Seville, J.P.K., "The dynamics of large particles in a four-compartment interconnected fluidized bed", *Powder Technol.*, **101**: 229–239 (1999).
50. Khalili, A., Basu, A.J. and Pietrzyk. U., "Flow visualization in porous media via positron emission tomography", *Phys. Fluids*, **10**(4): 1031–1033, 1998.
51. Khalili, A., Basu, A.J., Pietrzyk, U. and Raffel, M., "An experimental study of recirculating flow through fluid-sediment interfaces", *J. Fluid Mech.*, **383**: 229–247 (1999).
52. Hoff, W.D., Wilson, M.A., Benton, D.M., Hawkesworth, M.R., Parker, D.J. and Fowles, P., "The use of positron emission tomography to monitor unsaturated

water flow within porous construction materials", *J. Mat. Sci. Lett.*, **15**: 1101–1104 (1996).
53. Stellema, C.S., Vlek, J., Mudde, R.F., de Goeij, J.J.M. and van den Bleek, C.M., "Development of an improved positron emission particle tracking system", *Nucl Instrum Meth A*, **404**: 334–348 (1998).
54. Corte, H. and Dodson, C.T.J., Über die verteilung der massendichte in papier – erseter teil:theoretische grundlagen", *Das Papier*, **23**(7): 381–393 (1969).

## A REGIONS OF UNCERTAINTY IN THE MEASURED SIGNAL

In the ideal case, the interface between radioactive and non-radioactive material would be sharp. Expressed mathematically, the curvature in the signal would approach infinity at the interface. We attempt to locate the interface using the curvature in the data ($\kappa$) . If the measured 1D concentration profile is represented by the function $C(y, t)$, $\kappa$ is estimated using

$$\kappa = \frac{|C(y,t)''|}{[1 + (C(y,t)')^2]^{3/2}} \tag{31}$$

where the prime denotes differentiation with respect to $y$ An example of this is given in Figure 11 where we see two maxima located at the top of the sediment somewhere between pixels 83 and 89. The interface is smeared over this region and we are uncertain of the concentration profile in this region.

Further, for simplicity we assume that the interface is located halfway between the two peaks and use this to estimate the height of the sediment. We report the distance between the two peaks as the uncertainty in the measurement.

## B DERIVATION OF THE 1D FORCE BALANCE

At steady state, the fibres and fluid are at rest, i.e. $\boldsymbol{u} = \boldsymbol{w} = 0$. This implies that the inter-phase momentum term $\boldsymbol{M}$ is equal to zero, see Equation 8. With this, Equation 7 in one-dimension now reads

$$\frac{dP}{dy} = -\rho_w g \tag{32}$$

where $\boldsymbol{g} = (-g, 0, 0)$, which implies that the hydraulic pressure varies linearly with the sediment height. Upon substitution of this result into Equation 6 yields Equation 11.

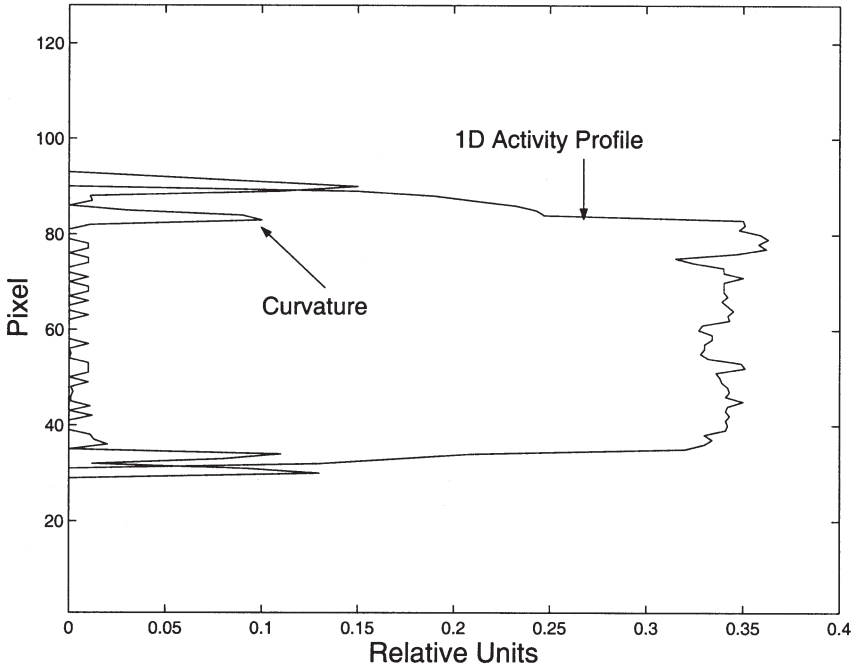


**Figure 11** A typical 1D projections from a 46 × 46 mm square subimage sampled from the middle of the container. The crowding number of the suspension was 10 and this image was taken at $t = 0.25$ min. The curvature at each point in the data is also shown as estimated from Equation 31. The edges of sediment are taken as the midpoint between the two large peaks. The distance between the two peaks is used as an estimate of the uncertainty.

## C DETERMINATION OF THE GEL POINT

With the second formulation, we begin the solution by scaling Equations 11 and 12 with

$$\Phi = \frac{\phi}{\phi_g} \tag{33}$$

$$Y = \frac{y}{h_s} \tag{34}$$

$$\epsilon = \frac{\Delta \rho g h_s}{mn\phi_g^{n-1}} \tag{35}$$

which gives

$$(\Phi - 1)^{n-1} \frac{\partial \Phi}{\partial y} = -\epsilon \Phi \tag{36}$$

$$\Phi_o = \frac{h_s}{H_o} \int_0^1 \phi dY. \tag{37}$$

These equations can be solved by a standard perturbation method as $\epsilon \ll 1$. If we express

$$\Phi = 1 + \epsilon^{1/n} \Phi_1 + \cdots \tag{38}$$

it turns out that

$$\Phi_1 = [n(1 - Y)]^{1/n}, \tag{39}$$

and

$$\Phi_o = \frac{h_s}{H_o} + \frac{n}{n+1} (n\epsilon)^{1/n} + \cdots, \tag{40}$$

Upon differentiation with respect to $h_s$, we end up with the same result as shown by Equation 16.

## Transcription of Discussion

# CHARACTERIZING THE MOBILITY OF PAPERMAKING FIBRES DURING SEDIMENTATION

*D.M. Martinez*[1,4], *K. Buckley*[2], *S. Jivan*[2], *A. Lindström*[1,4], *R. Thiruvengadaswamy*[1,4], *J.A. Olsen*[3,4], *T.J. Ruth*[2] *and R.J. Kerekes*[1,4]

[1]Department of Chemical and Bio-Resource Engineering, University of British Columbia
[2]TRIUMF, University of British Columbia
[3]Department of Mechanical Engineering, University of British Columbia
[4]The Pulp and Paper Centre, University of British Columbia

*Bill Sampson* Department of Paper Science, UMIST

How do you deal with air in the suspension? I have always found it a problem.

*Mark Martinez*

Air which occurs during sedimentation? That is a tricky point with mechanical pulp fibres air became a problem at high consistency and what we did was that we first shook it and then put it into a vacuum and removed the air. On some tests sedimentation was upwards because of the air. So in tests where sedimentation was downwards and we could not see any air bubbles we presumed that it was air free.

*Tom Browne* Paprican

I wonder if you could comment on the difference in sedimentation between long fibres which are stiff and undeveloped on the one hand long fibres which have been developed and are fibrillated and flexible. How would these types of fibre differ in sedimentation?

*Discussion*

*Mark Martinez*

I don't know

*John Daicic* Institute for Surface Chemistry, Stockholm

This is a nice piece of work. There is nothing in the number $N = 16$ which is related to the colloidal condition.

*Mark Martinez*

This is a problem, there is no physical reason at this point in time why $N = 16$ is significant. More work needs to be done.

*John Daicic*

So if you changed pH or another parameter would that affect $N = 16$ in some way?

*Mark Martinez*

I don't know, there are others who could answer the question better. Is it mechanical inter-locking or colloidal interaction. My belief is that it is mechanical but I do not want to venture down that road.

*John Daicic*

My other question was that on some of your graphs there is an expression called normalized time on your x-axis

*Mark Martinez*

That is the total length of time of the sampling

*John Daicic*

That relates to my question because in these systems you are a different distance away from equilibrium at comparable times, so in scaling your time there is no true scaling in that you have chosen an arbitrary total length of experiment time. I am wondering if it would be interesting to allow the system to settle to equilibrium and scale the entire graph by the sedimentation time in order to get a true scaled time.

*Mark Martinez*

That is a very good question, you are right this term relates to initial settling rates because we are away from the initial equilibrium position. The trouble is the half-life of the radioisotope. I had to choose an isotope with a length of time which could decay in a day but still give you enough time to actually do some experiments. Everything is just scaled to basically the half life of this fluorine, and my working time for this was maybe two hours at most.

*Dick Kerekes*

Mark is quite right, we haven't fully identified the physical significance of crowding number = 16, but we can hazard a guess as follows $N = 1$ represents occasional collisions amongst fibres, which is the crowding number of standard hand sheet forming and $N = 60$ represents where you have a three dimensional network with fibres locked into a bent configuration, where we know coherent flocks form. We suspect that $N = 16$ represents the conditions as which there are two contacts per fibre, which represents the onset of significant immobility. We, as Mark says, have not really confirmed this; but there does seem to a physical explanation. It requires further work to verify this.

*Kit Dodson* Department of Mathematics, UMIST

The equation of mine that you referred to was in fact produced in 1968 and published in 1969 the point that was very interesting to me was if you pursue what you described in linking these two expressions. K in our formula is actually known analytically for random deposition, and it is very interesting because there is also a precise formula for the analytic random three dimensional number of contacts, so there is a link here, that I was hoping that you would get to, but you didn't quite.

*Mark Martinez*

Well we are working on that right now and we are generating a large number of hand sheets with different length, or average length to see if we can actually compare your k to what we measure.

*Derek Page* Institute of Paper Science & Technology

I wonder if you would mind clarifying something for me. In the very last graph that you showed, everything was going fine until you came to that graph, and I said to myself, he is going to show us that all these data fall on

one line, and then they didn't. What is the meaning of the points being on different lines? Have I missed something?

*Mark Martinez*

No. It goes back to Prof. Dodson's comment that there is an inspection size involved here, and each one of these fibres have different lengths, OK, so if we knew what that function was, we could collapse it down to one line, and I wish I knew what that function was, but I just drew these, with different pulps and hand drew a line through them.

*Hannu Paulapuro* Helsinki University of Technology

You used one number to characterize formation did you try to include any formation distribution number also there? I think that if you are going to have shear forces, you may need to characterize formation by something else also.

*Mark Martinez*

Yes I completely agree with you, and I must reiterate a comment that Prof. Norman said to me, that we are measuring with 1 mm spot sizes. Something could be happening at a lower scale.

*John Parker* Consultant

I think in carrying out sedimentation experiments one must be very careful to avoid the effects of vibration, if one taps the size of the jar then the whole structure that one is sedimenting collapses, so in practice in a paper making machine one has vibrations, and I wonder what your comments are on this?

*Mark Martinez*

We did not perform this in a vibration free room, it was performed in the basement of a hospital in a tomograph. I personally did not find that if you tapped the side of the jar it would collapse more.

*Iikka Kartovaara* Stora Enso Oy

Some techniques have been developed for measuring the network strength for example by extracting the suspension from a tube into water. Have you made

any comparisons between your crowding number and those measured network strengths?

*Mark Martinez*

I'd like to address that question. No I have not done that. This type of analysis is typically called the inverse problem, i.e. solve the mass balance and force balance to find out what the network strength is. I did not do this in this work, I believe Prof. Kataja will be doing that at his presentation tomorrow or the next day.